AO15: The Refractive Index of Volcanic Ash Aerosols

Gavin Fourie
Supervisors: Dr D. Peters, Dr N. Bowles, and Dr R. Grainger

Abstract

This report demonstrates the use of a new method for determining the complex refractive index of solid aerosols, by their suspension in a Potassium Bromide medium. This is traditionally a difficult problem as the scattering of light from the aerosol particles must be accounted for. A quartz powder was used to verify the method. Band parameters and the complex refractive indices of quartz, and volcanic ash from the Eyjafjallajökull eruption of April 2010 in Iceland were obtained. In addition, the spectra of TiO_2, volcanic ash from the Grímsvötn eruption of May 2011 in Iceland, ash from the Mt Aso eruption of 1993 in Japan, Cape Verde dust, and JSC 1A (a moon dust simulant) were measured. All measurements were taken in the mid-infrared at wavenumbers between 400 and 8000 cm^{-1} (wavelengths between 1.25 and 25 μm).

1 Introduction

Satellite measurements of atmospheric aerosols are currently limited by a lack of knowledge of the optical properties of aerosols. Volcanic ash clouds can be identified by satellites through their spectral signatures, these signatures are in turn determined by the complex refractive index and the scattering properties of the ash. To date, a very limited range of ash refractive indices has been published and, furthermore, the ash from each eruption has a different composition. To improve the robustness of volcanic ash detection and the estimation of the aerosol mass loading in ash clouds, there is a need to quantify the range of possible refractive indices of volcanic ash. Improved knowledge of these refractive indices would allow volcanic ash clouds to be better characterised as to their location, the size and density of aerosol particles in the cloud, and the composition of the aerosols.

The eventual outcome is to better describe the location and possible danger that these clouds pose to aircraft [1].

2 Background

The method used to determine the refractive index of an aerosol was that of suspending the aerosol particles in a pellet of Potassium Bromide (KBr), and measuring the transmission through the pellet with a spectrometer. The measurements were then used in a retrieval scheme to obtain the refractive indices of the aerosol. Refractive indices are an intrinsic property of a substance, so the refractive indices derived herein are applicable to all situations where the aerosols occur.

When KBr powder is subjected to sufficient pressure, the powder fuses to produce a transparent window. KBr is used because it is softer than the aerosols so it does not distort the aerosol particles, KBr also has a nearly constant real refractive index and almost no absorption over the range investigated; the mid-infrared, at wavenumbers be-

tween 400 and 8000 cm^{-1} (wavelengths between 1.25 and 25 μm). Wavenumber, $\tilde{\nu}$, is related to wavelength, λ, by: $\tilde{\nu} = 1/\lambda$.

The real, n, and imaginary, k, parts of the refractive index of a substance describe how light is refracted and absorbed through that substance, respectively. For a plane wave travelling in a homogeneous medium with no scattering: [2]

$$\mathcal{E} = \mathcal{E}_{\mathbf{0}} \exp\left(-\frac{2\pi k x}{\lambda}\right) \exp\left(\frac{i2\pi n x}{\lambda} - i\omega t\right) \tag{1}$$

where x is the distance travelled through the medium, $\mathcal{E}$ is the electric field, $\mathcal{E}_0$ is the electric field at $x = 0$, λ is the wavelength of the light in vacuo, and ω is the angular frequency of the light. The Poynting vector, $\mathbf{S}$, for a wave propagating in the $\hat{\mathbf{e}}$ direction is therefore given by: [2]

$$\mathbf{S} = \frac{1}{2} Re\left\{\sqrt{\frac{\epsilon}{\mu}}\right\} |\mathcal{E}_{\mathbf{0}}| \exp\left(-\frac{4\pi k x}{\lambda}\right) \hat{\mathbf{e}} \tag{2}$$

where ϵ is the dielectric constant and μ is the permittivity, of the medium. The magnitude of the Poynting vector is the irradiance, $\mathcal{I}$, and it is attenuated as: [2]

$$\mathcal{I} = \mathcal{I}_0 e^{-\beta_{ext}(\tilde{\nu})x} \tag{3}$$

where $\beta_{ext}(\tilde{\nu})$ is the volume extinction coefficient; which for a homogeneous medium with no scattering is given by $\beta_{ext}(\tilde{\nu}) = 4\pi k/\lambda$, from eq. (2). However, light is scattered when it encounters particles, and therefore to accurately determine the refractive index we need to properly account for this scattering by modifying $\beta_{ext}(\tilde{\nu})$ (as in section 2.1) to include a scattering component.

A spectrometer was used to measure a spectrum of the sample pellet which was then divided by a spectrum of a background, pure KBr, pellet to obtain the transmission, $T(\tilde{\nu})$, though the sample pellet. The transmission is related to the volume extinction coefficient of the aerosol particles, $\beta_{ext}(\tilde{\nu})$, via the Beer-Lambert law: [2] [3]

$$T(\tilde{\nu}) = e^{-\beta_{ext}(\tilde{\nu})x} \tag{4}$$

where x is the thickness of the pellet and $\beta_{ext}(\tilde{\nu})$ contains the physical properties of the aerosol. The extinction, $E(\tilde{\nu}) = 1 - T(\tilde{\nu})$, was then used by the retrieval described in section 2.2 to obtain the complex refractive index of the aerosol.

2.1 Scattering

Mie theory is a solution to Maxwell's equations which describes the scattering of electromagnetic radiation in the case of spherical particles [2]. It is used when considering scattering by particles with dimensions comparable to the wavelength of light; Rayleigh scattering is the limiting case of Mie scattering for particles much smaller than the wavelength of light [3].

From Mie theory, the volume extinction coefficient, $\beta_{ext}(\tilde{\nu})$, at wavenumber $\tilde{\nu}$ of an aerosol population with a size distribution of $n(r)$ is given by: [4]

$$\beta_{ext}(\tilde{\nu}) = \int_0^\infty \pi r^2 Q^{ext}(\tilde{\nu}, m, r) n(r) dr \tag{5}$$

where Q^{ext} is the extinction efficiency as given by Mie theory; it is a function of complex refractive index, m, and the size parameter of the particle, $p = 2\pi r/\lambda = 2\pi r\tilde{\nu}$. If we assume a lognormal distribution of particle sizes: [5]

$$n(r) = \frac{N_0}{\sqrt{2\pi}} \frac{1}{\ln S} \frac{1}{r} \exp\left[-\frac{(\ln r - \ln r_m)^2}{2\ln^2 S}\right] \tag{6}$$

where N_0 is the total number density of particles, r is the radius of a particle, r_m is the median radius of the distribution, and the standard deviation of $\ln r$ is $\ln S$. Thus with a lognormal particle size distribution: [6]

$$\beta_{ext}(\tilde{\nu}) = \frac{N_0}{\ln S}\sqrt{\frac{\pi}{2}}\int_0^\infty rQ^{ext}(\tilde{\nu}, m, r) \times \exp[-\frac{(\ln r - \ln r_m)^2}{2\ln^2 S}]dr. \quad (7)$$

Therefore using the spectrometer measurements to obtain the transmission, and thereby $\beta_{ext}(\tilde{\nu})$, it is possible to determine Q^{ext}, which gives access to the complex refractive index, m.

2.2 The Forward Model

A retrieval method developed by Thomas et al. was used to obtain the refractive indices [6]. This method uses a classical damped harmonic oscillator (CDHO) model of molecular absorption and the Mie scattering theory to model extinction spectra, which are then fitted to measurements using the Levenberg-Marquardt numerical optimal estimation algorithm [6].

The CDHO model relates the complex dielectric constant, via the complex polarisability, to a set of q vibrational bands; each band is described by three band parameters, its intensity I_j, its width (damping constant) γ_j, and the oscillator's central wavenumber $\tilde{\nu}_j$, where $j = 0, 1, 2, ..., q$. The real, ϵ', and imaginary, ϵ'', parts of the dielectric constant for the material, are given in terms of the band parameters by:

$$\epsilon'(\tilde{\nu}) = \epsilon_\infty + \sum_j \frac{I_j(\tilde{\nu}_j^2 - \tilde{\nu}^2)}{(\tilde{\nu}_j^2 - \tilde{\nu}^2)^2 + \gamma_j^2\tilde{\nu}^2} \quad (8)$$

$$\epsilon''(\tilde{\nu}) = \sum_j \frac{I_j\gamma_j\tilde{\nu}}{(\tilde{\nu}_j^2 - \tilde{\nu}^2)^2 + \gamma_j^2\tilde{\nu}^2} \quad (9)$$

where ϵ_∞ is the value of the real part of the dielectric constant at infinite wavenumber (zero wavelength).

The real, n, and imaginary, k, parts of the refractive index are related to the dielectric constant by $n + ik = \sqrt{\epsilon' + i\epsilon''}$ [7] and are therefore given in terms of the dielectric constants as follows:

$$n(\tilde{\nu}) = \left(\frac{[\epsilon'(\tilde{\nu})^2 + \epsilon''(\tilde{\nu})^2]^{1/2} + \epsilon'(\tilde{\nu})}{2}\right)^{1/2} \quad (10)$$

$$k(\tilde{\nu}) = \left(\frac{[\epsilon'(\tilde{\nu})^2 + \epsilon''(\tilde{\nu})^2]^{1/2} - \epsilon'(\tilde{\nu})}{2}\right)^{1/2} \quad (11)$$

The forward model, $\mathbf{F}(\mathbf{x}) = \mathbf{y}$, relates the state vector, $\mathbf{x}$, to the measurement vector, $\mathbf{y}$, which in this case is given by the measured extinction values, $E(\tilde{\nu})$. The state vector, $\mathbf{x}$, consists of all the unknowns; m_∞, each band parameter (I_j, ν_j, γ_j) and the aerosol size distribution parameters (N_0, r_m, S). Where m_∞ is the relative refractive index of the aerosol to KBr at infinite wavenumber, from eq. (8) we see that $m_\infty = \sqrt{\epsilon_\infty}$. All the physics described in equations (4), (7), (8), (9), (10), and (11), i.e. scattering and the band model, is contained in the function $\mathbf{F}$. The quality of the fit, of $\mathbf{F}(\mathbf{x})$ to $\mathbf{y}$, is given by the probability of the state given the measurement, $P(\mathbf{x}|\mathbf{y})$. The Levenberg-Marquardt algorithm minimises the cost function below:

$$-2\ln P(\mathbf{x}|\mathbf{y}) = [\mathbf{y} - \mathbf{F}(\mathbf{x})]^{\mathbf{T}}\mathbf{S}_\epsilon^{-\mathbf{1}}[\mathbf{y} - \mathbf{F}(\mathbf{x})] + [\mathbf{x} - \mathbf{x_a}]^{\mathbf{T}}\mathbf{S_a^{-1}}[\mathbf{x} - \mathbf{x_a}] \quad (12)$$

where $\mathbf{S}_\epsilon$ is the error covariance matrix of $\mathbf{y}$, $\mathbf{x_a}$ is the a priori knowledge of the state before measurement and $\mathbf{S_a}$ is the covariance matrix giving the error in this knowledge.

The above description is credited to Thomas et al. [6] where full details of the retrieval used may be found.

3 Experimental Details

3.1 Synthetic spectrum

Tabulated data [8] for the refractive index of quartz was used with Mie scattering theory in a cut-down version of the forward model to produce a synthetic spectrum for quartz. Production of a synthetic spectrum serves two main purposes: to provide an initial estimate of the band parameters for quartz, and to estimate the mass of quartz powder to use in a pellet so as to get a good contrast in optical depth whilst maintaining a sufficiently high transmission. The model described in section 2.2 assumes a single scattering limit, where a photon which is scattered once is very unlikely to be scattered again and remain in the optical beam to be detected. The transition to a multiple scattering regime, where there is a significant probability of multiple scattering, occurs at an optical depth greater than approximately 1.0, i.e. at a transmission of less than e^{-1}.

Assuming the median radius, $r_m = 10.79\,\mu$m, obtained from the retrieval in a vacation project by Dreyer [9], and a spread of $S = 1.5$, I varied the number density used by the synthetic spectrum model to determine the approximate mass of quartz that gave a maximum optical depth of approximately 1.0 in the pellet. A quartz number density of $N_0 = 0.345 \times 10^6 \text{cm}^{-3}$ gave an optical depth of just less than 1.0. The density of quartz, $\rho_a = 2600\,\text{kg m}^{-3}$ [10], the radius, $r_p = 5\,$mm, and thickness, $x = 2\,$mm, of the pellet, and the assumption of a lognormal particle size distribution were required to determine the mass of aerosol, m_a, to be used in the pellet. It was found that a mass of 1.5 mg was required by use of the following equation: [5]

$$m_a = \frac{4}{3}\pi^2 N_0 x \rho_a r_m^3 r_p^2 \exp\left[\frac{9}{2}\ln^2(S)\right]. \quad (13)$$

See Appendix A for derivation.

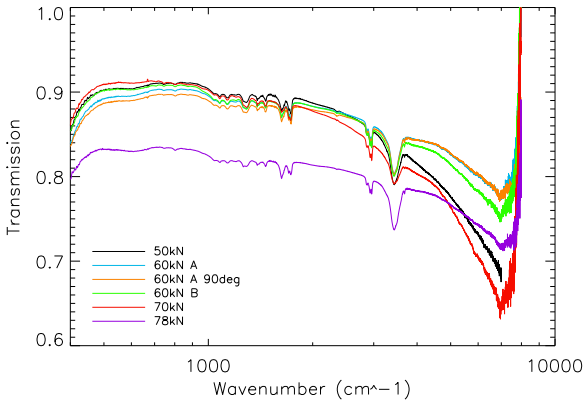

Figure 1: Spectra of pure KBr pellets (divided by a background with no pellet, so as to correct for the response of the spectrometer) manufactured at forces of 50 kN, 60 kN, 70 kN and 78 kN. The 60 kN A pellet was measured at a 90° axial rotation so as to determine the effect of pellet orientation.

3.2 Pellet Manufacture

Each pellet consisted of a 9 mm thick, 30 mm diameter stainless steel disc with an axial 10 mm diameter hole in the centre into which the sample, of KBr and aerosol particles, was pressed. A 10 tonne hydraulic press and a smaller bespoke die were used to press the pellets. The die had two pistons that pushed the pellet from above and below, creating a region of constant pressure in the centre, which contained the sample. The die was made from tooling steel, for hardness, and the surfaces of each piston were optically polished in order to give as good a surface to the KBr window as possible.

It was necessary to ascertain the force at which to press the pellets. If insufficient pressure was applied to the KBr this resulted in an opaque pellet, as the KBr powder did not fully fuse, causing excess scattering from the powder. A vacation project by Dreyer [9] demonstrated that the transmission was still increas-

ing at forces up to 30 kN, indicating that a greater force was required. I trialled a number of higher forces, and the results are shown in fig. 1. I discovered that for forces above 60 kN there was significant loss of sample around the sides of the piston, due to the sample escaping under the higher pressure. This appears to have led to a reduction in transmission, as seen for the whole wavenumber range of the 78 kN pellet and for wavenumbers above 1200 cm^{-1} of the 70 kN pellet. The 50 kN pellet also had a lower transmission in the range above 1200 cm^{-1} though this was more likely due to incomplete fusing at the lower pressure.

I decided to use a force of 60 kN to press the pellets containing the aerosol samples since this force gave the highest transmission and a good repeatability, as demonstrated by the 60 kN pellets A and B in fig. 1. In addition, I considered the effect of the axial orientation of the pellet in the spectrometer on the transmission. From fig. 1 we can see that the orientation does not appear to have a large affect on the spectrum, and the effect is smaller than the difference in repeatability of different pellets pressed with the same force. However, so as to be as accurate as possible, I ensured that all further pellets were made with the press oriented in the same direction and that the measurements were all taken at the same axial rotation.

All KBr and aerosol samples were dried in a vacuum oven overnight before pressing them into the pellets, in order to remove any excess water. In addition, whenever washing the stainless steel discs in water they were left in the oven to dry overnight. Between making each pellet, the dies were washed in an ultrasonic bath with high purity Propan-2-ol (IPA), to ensure there was no contamination between pellets. The dies were then dried in the oven for one hour.

For each pellet I used between 0.45 and 0.5 g of KBr, as suggested by Dreyer [9], with approximately 1.5 mg of aerosol particles, as determined in section 3.1. The masses of the aerosol and KBr used were recorded, and the powders were mixed together in a glass beaker using a steel rod. I had intended to use a porcelain pestle and mortar, however, I found that this contaminated the samples. I used the same mass of volcanic ash as quartz powder because the volcanic ash is likely to contain a reasonably high proportion of quartz, and no other data for the volcanic ash were available. After pressing each pellet to 60 kN, I measured the thickness of the pellet with digital vernier callipers. The thickness varied from 1.86 mm to 2.17 mm.

All pellets were stored in an air tight container with a sachet of silica gel to desiccate the air. Each pellet had kapton tape placed over both sides of the hole that contained the sample, to prevent the sample surfaces becoming dusty. It was very important to place the pellets in a desiccated environment quickly since one pellet left on the balance for an hour went opaque, probably due to water uptake, and could not be used for measurements.

3.3 Pellet Measurement

A Bruker Fourier-Transform Infra-red spectrometer using a KBr beamsplitter, with a Globar mid-infrared source, and a 5 mm aperture was used to measure the spectra. Measurements of a pure KBr pellet, as the background, were taken before and after taking measurements of the sample. Each spectral measurement consisted of an average of 50 scans and was repeated 10 times over half an hour.

The mean of the sample spectra was divided by the mean of the background, pure KBr, spectra to obtain the transmission, $T(\tilde{\nu})$, of the aerosol sample in the pellet; which is related to the aerosol volume extinction coefficient, $\beta_{ext}(\tilde{\nu})$, by eq. (4).

Since the pellets were of different thicknesses

and the KBr itself has a volume extinction coefficient, $\beta_{KBr}(\tilde{\nu})$, the implications of this on the measured spectra must be considered. Let A_{a+KBr} be the spectrum of the aerosol pellet with a thickness of x, A_{KBr} be the spectrum of the pure KBr pellet with a thickness of x_2, and $T(\tilde{\nu})$ be the final transmission through just the aerosol sample, corrected for the KBr background and the wavelength dependency of the spectrometer:

$$A_{a+KBr} = B(\tilde{\nu})e^{-\{\beta_{ext}(\tilde{\nu})+\beta_{KBr}(\tilde{\nu})\}x} \quad (14)$$

$$A_{KBr} = B(\tilde{\nu})e^{-\beta_{KBr}(\tilde{\nu})x_2} \quad (15)$$

where $B(\tilde{\nu})$ represents the response of the spectrometer, which depends on the source, beam splitter, detector etc.

Dividing (14) by (15) we obtain:

$$T(\tilde{\nu}) = e^{-\beta_{ext}(\tilde{\nu})x-\beta_{KBr}(\tilde{\nu})x\{1-\frac{x_2}{x}\}} \quad (16)$$

We find that $\beta_{KBr}(\tilde{\nu})$ is small (since KBr is a solid homogenous material with negligible scattering, $\beta_{KBr}(\tilde{\nu}) = 4\pi k/\lambda$ [2], and the largest tabulated value in the mid-infrared for k is 1.2×10^{-5} at $450\,\mathrm{cm}^{-1}$ [8]) and x_2/x is very close to unity. We can therefore make the approximation of neglecting the $\beta_{KBr}(\tilde{\nu})$ term so that we recover the equation for transmission, eq. (4):

$$T(\tilde{\nu}) = e^{-\beta_{ext}(\tilde{\nu})x}. \quad (17)$$

In addition, we make the approximation that the surface reflectivity of the pure KBr pellet and the aerosol pellet are the same, thereby when dividing the two, the reflectivities cancel out; this is reasonable as the vast majority of the material in both pellets is KBr and they were all manufactured and measured in the same manner.

Table 1: Table of Quartz band parameters, the corresponding aerosol parameters are $m_\infty = 0.99554$, $N_0 = 118.80$, $r_m = 0.438\,19\,\mu\mathrm{m}$, $S = 2.7538$. All numbers given are rounded to 5 significant figures.

$\tilde{\nu}(\mathrm{cm}^{-1})$	$\gamma(\mathrm{cm}^{-1})$	$I(\mathrm{cm}^{-2})$
465.33	20.298	39134
508.37	24.147	10806
695.66	7.0652	1608.6
789.58	19.241	21069
1075.3	37.765	183130
1157.2	71.099	54148

3.4 Particle Size, Spread and Number Density

In addition to the band parameters described in section 2.2, the retrieval scheme also required a priori information on the particle size, spread and number density. To obtain this information I used an aerosizer at the Rutherford Appleton Laboratory (RAL) to measure the aerodynamic diameter distribution of the samples. The aerodynamic diameter is the diameter of a water droplet with the same aerodynamic properties of the sample particle. If we assume that our particles are spheres this aerodynamic diameter can be converted into a geometric diameter via the relation: [11]

$$d_{geometric} = d_{aerodynamic}\left(\frac{\rho_0}{\rho_p}\right)^{1/2} \quad (18)$$

where ρ_0 is the density of water and ρ_p is the density of the sample particles.

The number density of aerosol particles in the pellet was calculated by eq. (13) using the measured radius, $r_m = d_{geometric}/2$, the spread, and the known mass of aerosol in each pellet.

See Appendix B for the measured size distribution of the quartz powder, and the Eyjafjallajökull ash.

Table 2: Table of Eyjafjallajökull ash bands, the corresponding aerosol parameters are $m_\infty = 0.99882$, $N_0 = 19.908$, $r_m = 1.0941\,\mu$m, $S = 1.7047$. Note that the width of the first band and the intensity of the sixth band have hit the hard lower limits specified in the retrieval, this is undesirable however appears to be required to obtain a reasonably close fit for the measured spectrum. With the exception of the two numbers mentioned above all numbers given are rounded to 5 significant figures.

$\tilde{\nu}(\text{cm}^{-1})$	$\gamma(\text{cm}^{-1})$	$I(\text{cm}^{-2})$
339.42	0.00010	158370
392.96	64.786	95385
436.96	99.024	63855
573.36	188.72	104260
736.38	117.18	47490
812.94	1303.7	0.00010
975.95	101.95	430530
1120.6	182.38	106080
1513.4	1372.5	315800
3403.6	420.73	82733

3.5 Refractive Index Retrieval

I made use of the retrieval scheme developed by Thomas et al. [6] which retrieves the complex refractive index of a material from a spectrum, as described in section 2.2. This required the input of a 'first guess' of the state vector, $\mathbf{x}$, which contains the particle size distribution and band parameters for the material. In addition, a priori knowledge of these parameters and their uncertainty is included in the vector $\mathbf{x_a}$ and the associated error matrix $\mathbf{S_a}$. Ideally the a priori parameters would be taken from existing published data.

To obtain an initial estimate for the band parameters of quartz I used the retrieval scheme on the synthetic quartz spectrum from section 3.1. This was achieved by starting with the band parameters determined by Spitzer et al. [12] for the o-ray and e-ray of quartz. Since quartz powder, which contains randomly oriented particles, was used, these bands were not an exact match and some of the bands were shifted in wavenumber. After a number of attempts I obtained a fit which was reasonably close to the synthetic spectrum. I applied these bands, along with the measured particle size distribution, as the first guess and a priori information to the measured quartz pellet. By again adjusting the bands I was able to obtain a close fit for the observed quartz spectrum. The final bands are given in table 1.

To the best of my knowledge there exist no published band parameters for any volcanic ash; consequently I used the band parameters obtained from the synthetic spectrum of quartz as a first step in the retrieval of the refractive indices of Eyjafjallajökull ash. A number of additional bands were required so as to correctly represent the extinction spectrum. The final band parameters used to calculate the refractive indices for Eyjafjallajökull volcanic ash are given in table 2.

The retrieved refractive index is the relative refractive index of the sample to the refractive index of the KBr medium ($n_{KBr} + ik_{KBr}$):

$$m = \frac{n + ik}{n_{KBr} + ik_{KBr}} \tag{19}$$

where n and k are the real and imaginary parts of the refractive index of the aerosol sample, respectively, and m is the retrieved complex refractive index. The final refractive index of the aerosol was obtained by multiplying the retrieved refractive index by the complex refractive index of KBr.

4 Results

As can be seen from the Grímsvötn May 2011 ash in fig. 2b some of the pellets did not work as expected, the transmission clearly should not be higher than 1.0. Here it seems that the

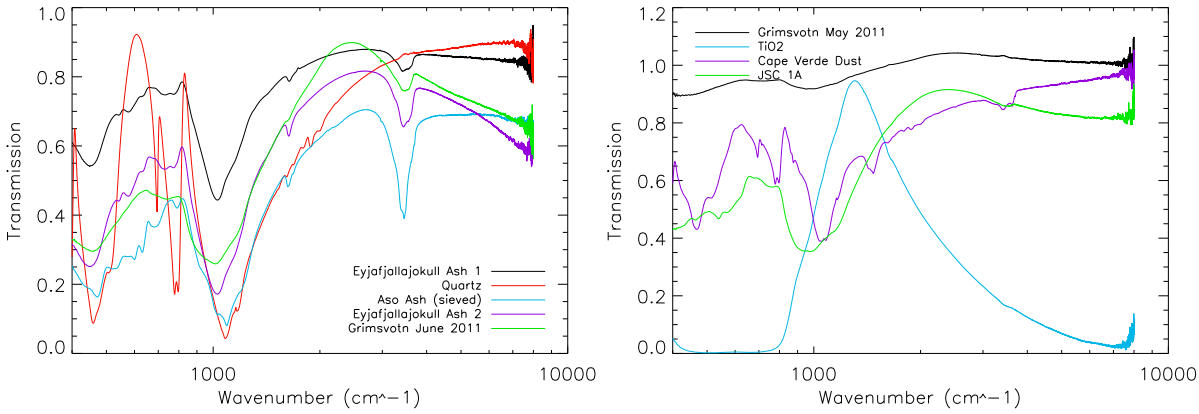

(a) (b)

Figure 2: Spectrum (a) shows Eyjafjallajökull ash from the eruption of April 2010 in Iceland (1 and 2 are the same sample but different pellets), Mt. Aso ash from the eruption of 1993 in Japan sieved to $<22.5\,\mu$m, Grímsvötn ash from the eruption of 2011 in Iceland (collected 200 m from the vent in June 2011), and Quartz powder. Spectrum (b) shows Grímsvötn ash from the eruption of 2011 in Iceland (collected in May 2011), Titanium dioxide (TiO_2), dust from the Cape Verde Islands (a loess, wind blown silt, sample deposited from the Saharan region over many thousands of years), and JSC 1A (a moon dust simulant).

spectrometer has drifted significantly over the measurement period, it is also possible that the ash was not sufficiently well mixed into the KBr powder. The TiO_2 pellet, in fig. 2b, shows almost no transmission between 400 and 800 cm^{-1} indicating that too much TiO_2 powder was used in the pellet.

The refractive indices obtained from the quartz spectrum, in fig. 2a, are shown in fig. 3a and fig. 3b.

I decided to focus on analysing the spectrum of Eyjafjallajökull Ash 1, in fig. 2a, as it had the highest transmission of the ash spectra (excluding Grímsvötn May 2011, which appears to be anomalous) and was therefore the least likely to be significantly affected by multiple scattering, which the current retrieval does not take into account. The refractive indices obtained for Eyjafjallajökull volcanic ash are given in fig. 4a and fig. 4b.

The standard deviations of the sample pellet spectra were used to estimate the random error in the measurements, as shown in fig. 5b. Fig. 5a shows that systematic shifts in the background data (the difference between measurements taken before and after the sample pellet data) produced errors up to an order of magnitude greater than the random error. Due to time and equipment limitations, to attempt to account for this large systematic error I was advised to increase the random errors by an order of magnitude to give a rough estimate of the errors on the final result. This is not a rigorous error analysis but does give some handle as to the errors. Thus the errors presented in fig. 4a and fig. 4b give an estimate of the likely errors on the refractive indices, but must be treated with caution.

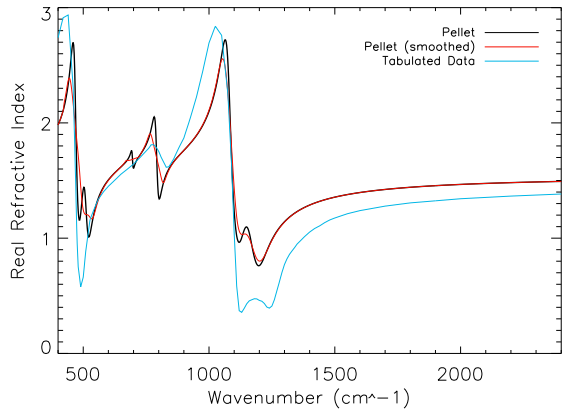

(a) Real Refractive Index

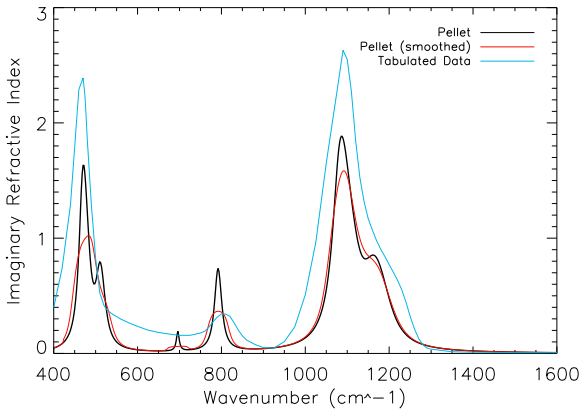

(b) Imaginary Refractive Index

Figure 3: Real (a) and imaginary (b) parts of the refractive index of quartz, the smoothed data is the measured values smoothed with a boxcar smoother of width $25\,\mathrm{cm}^{-1}$, and tabulated data is from the Handbook of optical constants of solids [8]. Data presented here are derived from the closest fit obtained in the retrieval. No errors are plotted as the errors produced by the retrieval are so small here that they aren't visible, this demonstrates that the errors are likely being underestimated.

5 Discussion

The spectra in fig. 2a and fig. 2b mostly give a satisfactory variation in transmission, making the main absorption bands relatively easy to spot (important for the retrieval). The two Eyjafjallajökull pellets, whilst having different magnitudes of transmission, look very similar with all the same bands present, which is encouraging as to the repeatability and reliability of the experiment.

From fig. 3a and fig. 3b we see that the position of peaks in the refractive indices of quartz generally agree with the tabulated data, however, they are not the same. One of the possible reasons for this is the lower resolution of the published data. In order to better compare the pellet data and the published data I smoothed out the quartz pellet data using a boxcar smoother at about the resolution of the published data ($25\,\mathrm{cm}^{-1}$), though the resolution of the published data does vary over the range displayed. It is interesting to note that the peak at about $700\,\mathrm{cm}^{-1}$ in fig. 3b is very small in the smoothed data, and thus a lower resolution experiment may not have detected it, though I cannot exclude the possibility that this peak in the pellet data is an artefact of the experiment. The smoothed pellet data appears to be quite similar to the tabulated data in shape, however, the magnitude is clearly very different. The tabulated data presented by Palik [8] were derived from a number of different papers and unfortunately the errors are not known on either the tabulated data or my quartz pellet data, so it is not possible to state definitively if they agree or disagree within the errors. The refractive index of the quartz seemed to be quite strongly dependent on the retrieval and varied in magnitude quite significantly with different assumptions and starting points, so this could be a large source of errors on my quartz refractive indices; this is in contrast to the Eyjafjallajökull re-

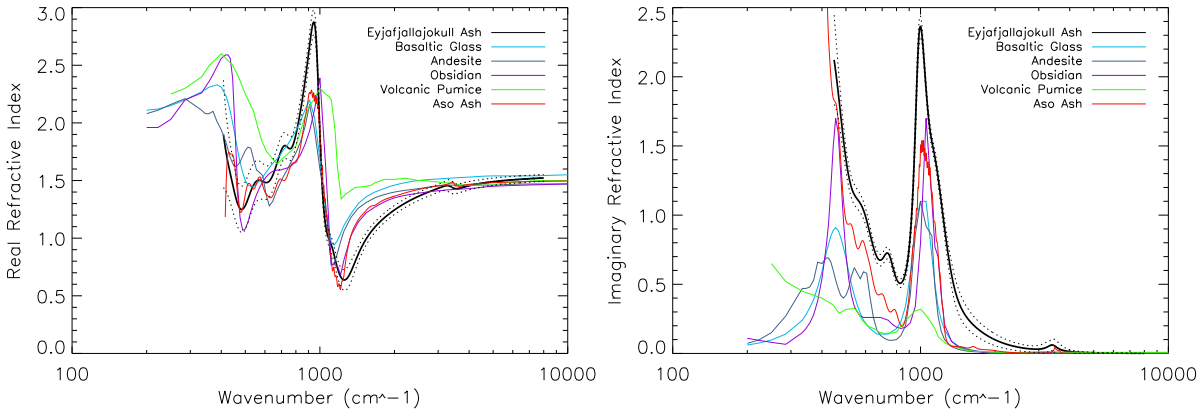

(a) Real Refractive Index

(b) Imaginary Refractive Index

Figure 4: Real (a) and imaginary (b) parts of the refractive index of Eyjafjallajökull ash with refractive indices for basaltic glass, andesite and obsidian from Pollack et al. [13], for volcanic pumice from Volz [14], and for Aso ash from Grainger et al. [15]. The black dotted lines display one standard deviation of the estimated errors on the measured data. Data presented for Eyjafjallajökull ash excludes values at wavenumbers below which the error bars began to diverge.

fractive indices which were more stable against changes in the retrieval.

Both the real and imaginary parts of the refractive index of Eyjafjallajökull ash in fig. 4a and fig. 4b match up well with the currently published data for various volcanic materials, though the peaks at $1000\,\mathrm{cm}^{-1}$ do appear to be significantly larger than the other volcanic materials. It is important to note that the other refractive indices in these plots, except the Aso ash, are not volcanic ash. Whilst it is reasonable to compare the results from this experiment to the other volcanic materials, we would not necessarily expect them to be identical, especially since different volcanoes have different mineralogies and thus different refractive indices. The fact that these refractive indices are similar makes the data much more useful to ash cloud detection regimes, since if they were all significantly different it would not be possible to generalise to future ash clouds of unknown mineralogies.

5.1 Further Work

It became clear that some of the volcanic ash pellets did not produce the expected spectra, this was probably due to the large particle size of some of the ash samples (and possible presence of agglomerates). Due to contamination of the samples when attempting to use a porcelain pestle and mortar, it was not possible to grind and mix the samples to a satisfactory degree. The laboratory is therefore considering the purchase of a zirconium oxide pestle and mortar; this material is exceptionally hard, and in particular harder than quartz, thus avoiding contamination of the samples. A Zirconium pestle and mortar would allow the ash samples to be ground, to remove agglomerates, and mixed more effectively, so as to disperse the smaller particles more evenly throughout the KBr.

Quantification of the systematic errors caused by the spectrometer drift was curtailed

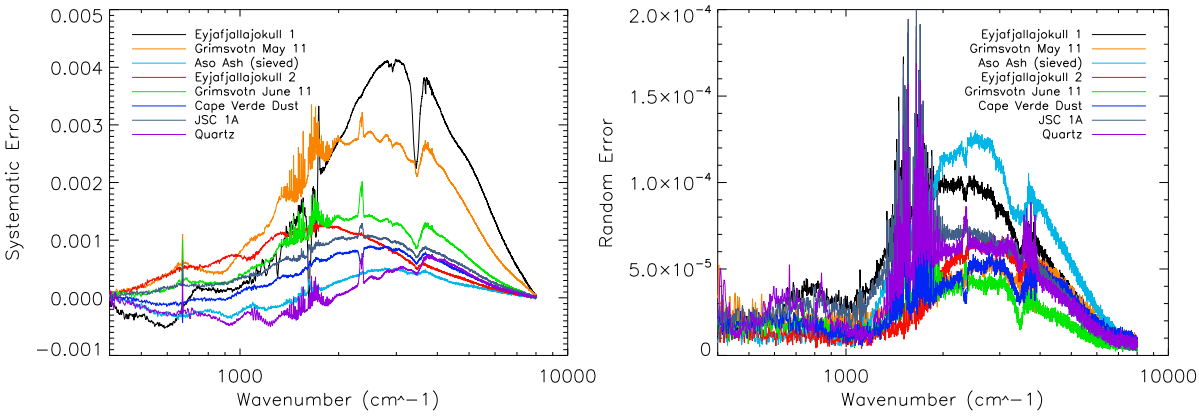

(a) Systematic Errors

(b) Random Errors

Figure 5: The systematic errors (a) were derived by finding the difference between measurements of the background, pure KBr, pellet measurements taken before and after the sample pellet measurement. The random errors (b) were found by taking the standard deviation of each of the sample pellet measurements. The errors of TiO_2 are not shown as they are much larger due to the very small transmission through that sample pellet.

as it was not possible to run the spectrometer overnight, due to the possibility of the vacuum pump malfunctioning. Ideally, one would want to run the spectrometer for a significant period of time in order to characterise its systematic drift. The large systematic error appears to be mostly due to the drift in the spectrometer and it is likely that, in part, this is due to variations in the ambient temperature of the laboratory. It would therefore be helpful to attempt to stabilise the ambient temperatures, possibly by tighter control of the air conditioning system. Drift can also be caused by shifts in instrument alignment and so making use of the Molecular Spectroscopy Facility at RAL would be useful in this regard, as it would provide a more stable and reliable instrument which could be run for an extended period of time. This would both reduce, and increase ones ability to quantify, the systematic errors; which could then be combined with the random error term by adding the errors in quadrature (assuming the errors are normally distributed and independent). The total error could then be included in the retrieval so as to give a much more rigorous account of the errors on the obtained refractive indices.

A different beam splitter, with a different spectral response, could be used to extend this method. This would allow the refractive indices to be determined over a wider range of wavelengths, which would further improve the utility of the data to ash cloud detection regimes.

The current retrieval scheme has a number of limitations, the most significant of which are that the model: does not take account of multiple scattering, assumes a single log-normal size distribution, and assumes spherical particles. To get a reasonable signal response in the spectrometer requires a sufficient number of particles in the sample, yet as the number of particles increases the probability of multiple scattering increases. The retrieval algorithm could therefore be extended to include multiple scattering. Many of the sam-

ples exhibited a bimodal lognormal size distribution, the model could either be extended to deal with a bimodal distribution or, preferably, it could be modified to include the actual measured size distribution as an input. The sphericity of our ash and other samples is unknown, and since (as discussed in section 2.1) Mie scattering assumes spherical particles this could be a significant source of error. There exists a model which accounts for non-spherical particles, called T-matrix scattering [15], which would offer an improvement in this regard. These modifications to the retrieval scheme would likely come at the cost of computing speed, by adding additional complexity to the model. This could be a significant disadvantage since the retrieval can already take a number of hours to run; however, these improvements would likely more accurately model the observed spectrum and reduce the errors which are associated with the retrieval scheme.

The best experiment for measuring the refractive index of aerosols is to directly measure the particles dispersed in air, as this is how they naturally occur in the atmosphere. Whilst this presents many of its own difficulties it is a logical next step to better characterise the optical properties of volcanic ash.

6 Conclusion

This project has resulted in the successful manufacture of pellets, and their measurement by use of a spectrometer. Via inversion of these measured spectra, the identification of band parameters for quartz and Eyjafjallajökull volcanic ash has been achieved. The complex refractive indices of quartz, and of ash from the Eyjafjallajökull eruption of April 2010 in Iceland have been obtained and, whilst the errors on these data still require some further work to fully determine, the results largely agree with pre-existing data for other similar substances. This project has further validated and significantly developed the method of determining refractive indices by suspending particles in a Potassium Bromide medium, and it is hoped that this work can be built upon in the future to obtain refractive indices for a wider range of wavelengths and substances.

Acknowledgements

Many thanks must go to my supervisor Dan Peters for his exceptional help throughout this project, Don Grainger for his steadying hand and wise guidance, Neil Bowles for his advice and support, and Ian Thomas for his help in coercing the spectrometer to work.

References

[1] R. G. Grainger and J. J. Barnett. Using the high resolution and dynamics limb sounder (hirdls) to warn aviation of volcanic ash. Oxford, 1997.

[2] Craig F. Bohren and D.R. Huffman. *Absorption and scattering of light by small particles*. Wiley science paperback series. Wiley, 1983.

[3] D.G. Andrews. *An Introduction to Atmospheric Physics*. Cambridge University Press, 2010.

[4] Roy G. Grainger, Jonathan Lucas, Gareth E. Thomas, and Graham B. L. Ewen. Calculation of mie derivatives. *Optical Society of America*, 2004.

[5] R. G. Grainger. *Some Useful Formulae for Aerosol Size Distributions and Optical Properties*. http://www.atm.ox.ac.uk/user/grainger/research/aerosols.pdf. Last accessed: 12/03/2012.

[6] Gareth E. Thomas, Stephen F. Bass, Roy G. Grainger, and Alyn Lambert. Retrieval of aerosol refractive index from extinction spectra with a damped harmonic-oscillator band model. *Optical Society of America*, 2005.

[7] John E. Bertie, Shuliang L. Zhang, and C.Dale Keefe. Infrared intensities of liquids xvi. accurate determination of molecular band intensities from infrared refractive index and dielectric constant spectra. *Journal of Molecular Structure*, 324(1–2):157 – 176, 1994.

[8] E.D. Palik and G. Ghosh. *Handbook of optical constants of solids*. Handbook of Optical Constants of Solids. Academic Press, 1998.

[9] Frédéric Dreyer. Vacation project, iaeste internship. Supervised by N. Bowles, Oxford, 2011.

[10] International Programme on Chemical Safety Inchem. Quartz. http://www.inchem.org/documents/icsc/icsc/eics0808.htm. Last accessed: 13/03/2012.

[11] William C. Hinds. *Aerosol Technology*. Wiley-Interscience, 1999.

[12] W.G. Spitzer and D. A. Kleinman. Infrared lattice bands of quartz. *Physical Review*, 121(5), 1961.

[13] James B. Pollack, Owen B. Toon, and Bishun N. Khare. Optical properties of some terrestrial rocks and glasses. *Icarus*, 19(3):372 – 389, 1973.

[14] Frederic E. Volz. Infrared optical constants of ammonium sulfate, sahara dust, volcanic pumice, and flyash. *Applied Optics, 12, 564–568*, 1973.

[15] R.G. Grainger, D.M. Peters, G.E. Thomas, A. Smith, R. Siddans, E. Carboni, and A. Dudhia. Measuring volcanic plume and ash properties from space, in remote sensing of volcanoes and volcanic processes: Integrating observation and modelling. *The Geological Society Special Publication 270*, submitted. D.Pyle and T. Mather (eds).

Appendices

A Derivation of aerosol mass equation

The total volume of a pellet of thickness, x, and radius, r_p, is given by:

$$V_{pellet} = \pi r_p^2 x. \tag{20}$$

The volume of the pellet consists of a contribution from both the aerosol and the KBr medium:

$$V_{pellet} = V_{aerosol} + V_{KBr}. \tag{21}$$

Following Grainger [5] and assuming a lognormal size distribution of the aerosol particles, the volume density (the volume of aerosol particles per unit volume of pellet) is given by:

$$V_{density} = \frac{4}{3}\pi N_0 r_m^3 \exp\left[\frac{9}{2}\ln^2(S)\right] \tag{22}$$

where N_0 is the aerosol number density, r_m is the median aerosol radius, and S is the spread (the standard deviation of $\ln r$ is $\ln S$). The volume of the aerosol in the pellet is therefore:

$$V_{aerosol} = V_{density} \times V_{pellet}. \tag{23}$$

Which gives:

$$V_{aerosol} = \frac{4}{3}\pi N_0 r_m^3 \exp\left[\frac{9}{2}\ln^2(S)\right] \times \pi r_p^2 x. \tag{24}$$

The mass of the aerosol in the pellet is then given by:

$$m_a = \rho_a V_{aerosol}. \tag{25}$$

Therefore, the mass of aerosol to use in a pellet for a given N_0 is:

$$m_a = \frac{4}{3}\pi^2 N_0 x \rho_a r_m^3 r_p^2 \exp\left[\frac{9}{2}\ln^2(S)\right]. \tag{26}$$

To work out the mass we require ρ_a, which is well documented, we also require x, r_m, and S.

B Measured aerosol size distribution

These size distributions were measured on the aerosizer at RAL as described in section 3.4.

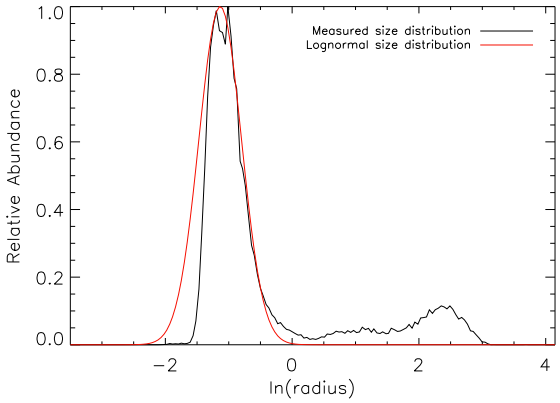

Figure 6: Measured size distribution of quartz powder, with the red line showing a fitted lognormal function with a median radius, $r_m = 0.36\,\mu$m and a spread, $S = 1.4$.

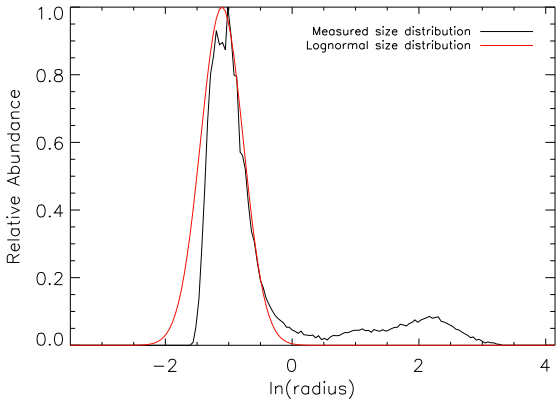

Figure 7: Measured size distribution of Eyjafjallajökul ash, with the red line showing a fitted lognormal function with a median radius, $r_m = 0.37\,\mu$m and a spread, $S = 1.4$.